caused by errors in the LIF method or in the subsequent data analysis.

Figure 4 shows data, at low F, for $Q_1(N'')$ and $R_1(N'')$. The unusual structure of the R_1 branch has already been noted. In contrast, the Q_1 branch is reasonably Boltzmann-like and yields a temperature of ≈580 K. As was pointed out in the experimental section, we cannot deduce absolute λ doublet population ratios $(\pi^-/\pi^+) \equiv \phi$ from our data. However, there is a big decrease in ϕ at larger N''. Because it is likely, particularly at high F, that the OH that have larger N'' are thermalized, it seems plausible to assume that $\phi \approx 1$ there. If this is correct, it implies a preponderance of the π^- state in nascent OH at low N''.

We have similar results and conclusions with $Q_2(N'')$ and $R_2(N'')$ at low F. However, because of line overlaps in the Q_2 branch, we feel more secure with $Q_1(N'')$ and $R_1(N'')$.

Conclusions

The main point here is to show the existence of these unusual population distributions and to encourage further work. The present "low F" results do not represent nascent OH, because the population ratios $R_2(2)/R_2(3)$ are still changing at even lower F.

There is no reason why better experiments cannot be designed that (a) use smaller F, (b) operate at closer probe–target distances, and (c) use a detection system whose response to polarized light is known, so that absolute λ doublet populations can be deduced. Another interesting study would be the correlation of rotational states with translational energies.

Finally, once the experimental facts are established, an explanation should be sought for the origin of such fine structure in the distributions. Because this depended so sensitively upon initial conditions in H_2O, we did not attempt even a qualitative interpretation.

Acknowledgment. E.W.R. was Richard Bernstein's first graduate student in the molecular beam area (1955–59). He gratefully acknowledges the privilege of having worked with Bernstein as his student, as a colleague, and as a friend. Bernstein was a continuing inspiration, and he is sorely missed. We thank the donors of the Petroleum Research Fund, administered by the American Chemical Society, and the WSU Institute for Manufacturing Research for partial support of this work.

Registry No. $Ca(OH)_2$, 1305-62-0; OH, 3352-57-6.

Effect of Surface Temperature on Collision-Induced Dissociation of *i*-C_3F_7NO Scattered from MgO(100), GaAs(100), and Ag(111)†

P. S. Powers,‡ E. Kolodney,§ L. Hodgson,∥ G. Ziegler, H. Reisler,* and C. Wittig*

Department of Chemistry, University of Southern California, Los Angeles, California 90089-0482
(Received: March 26, 1991; In Final Form: June 7, 1991)

The surface temperature (T_s) dependence of hyperthermal molecule–surface collision-induced dissociation (CID) was studied at incident kinetic energies of 1–5 eV and T_s = 300–760 K. *i*-C_3F_7NO was impulsively scattered from MgO(100), GaAs(100), and Ag(111) single crystals under ultrahigh vacuum conditions. CID yields, as well as internal energy distributions, were obtained for the product NO fragment, employing state-selective laser ionization detection. CID yields were found to increase strongly with T_s, whereas NO rotational and spin–orbit excitations were relatively insensitive to T_s. The CID yield was largest for scattering *i*-C_3F_7NO from MgO(100) and smallest for Ag(111). It is shown experimentally that surface morphology and stoichiometry do not change significantly with T_s in the range studied here. The experimental results are rationalized in terms of coupling of the translational motion of the incident molecule to surface phonons.

I. Introduction

The direct inelastic scattering of a molecule from a single-crystal surface constitutes one of the most basic processes in gas–surface interactions and is quite often the initial entrance channel step for more complicated reactive processes. Understanding the dynamical details of the mechanisms involved, as well as their dependence upon initial conditions, is prerequisite to obtaining a detailed understanding of more complex processes whose evolution is influenced by the molecule–surface excitations and deformations brought about by the impulsive collision. Recently, considerable attention has been devoted to molecule–surface scattering, with emphasis on energy transfer from the translational energy of the incoming molecule into crystal vibrations and internal degrees of freedom of the scattered molecule. In particular, several important direct processes have been observed for polyatomic molecules scattered from MgO(100)[1] and diamond(111),[2-4] including intramolecular excitations, collision-induced dissociation (CID) where one of the fragments is an atom (i.e., I) or an open-shell molecule (i.e., NO), ionization, dissociative ionization, and energy transfer to the crystal.

By their nature, the time scales for impulsive particle–surface interactions are very short, with memory of the incident momentum fully or partially retained. Quite often the surface, as seen by the rapidly approaching molecule, appears to be "vibrationally frozen" on the collision time scale; hence, some of the observables are not expected to be sensitive to the surface temperature. However, it should be pointed out that the effect of surface temperature in direct inelastic processes depends upon the nature and properties of the surface as well. For metallic surfaces, bulk temperature controls the density of charge carriers, and molecule–surface electronic interactions are expected to be sensitive to these changes and exhibit corresponding dependences.

† Research supported by AFOSR and the ARO Center for the Study of Fast Transient Processes.
‡ Department of Education Predoctoral Fellow.
§ Present address: Technion Institute of Technology, Haifa, Israel.
∥ NSF Predoctoral Fellow.

(1) Kolodney, E.; Powers, P. S.; Hodgson, L.; Reisler, H.; Wittig, C. *J. Chem. Phys.* **1991**, *94*, 2330.
(2) Danon, A.; Kolodney, E.; Amirav, A. *Surf. Sci.* **1988**, *193*, 132.
(3) (a) Danon, A.; Amirav, A. *J. Phys. Chem.* **1989**, *93*, 5549. (b) Amirav, A. *Comments At. Mol. Phys.*, submitted. (c) Danon, A.; Amirav, A. *Isr. J. Chem.* **1989**, *29*, 443.
(4) Danon, A.; Amirav, A.; Silberstein, J.; Salman, Y.; Levine, R. D. *J. Phys. Chem.* **1989**, *93*, 49.

0022-3654/91/2095-8387$02.50/0

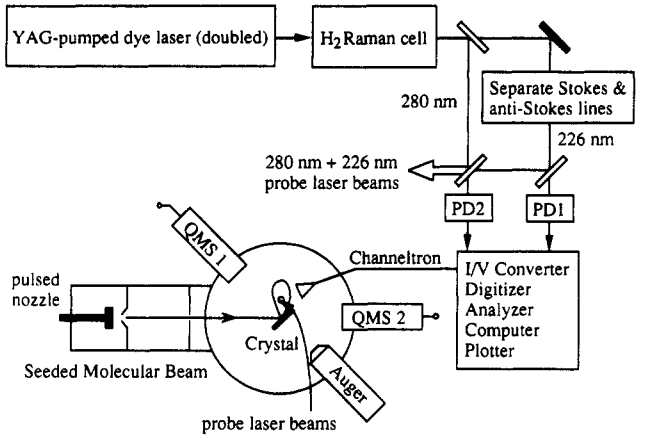

Figure 1. Schematic drawing of the experimental arrangement used in the molecule–surface CID studies.

Such a mechanism was recently used to explain the strong temperature dependence observed for $v'' = 1$ vibrational excitation of NO impulsively scattered from Ag(111).[5] However, on insulating surfaces, this mechanism is unlikely to dominate. Other possible sources of surface temperature effects may be phonon excitations or changes in the surface morphology and/or stoichiometry upon heating.

In this paper, we report the CID of i-C_3F_7NO scattered from MgO(100), GaAs(100), and Ag(111) surfaces, with particular emphasis on the effect of surface temperature on dissociation yields. For all three surfaces, the main dependence found was an increase of the dissociation yield with surface temperature, T_s. For i-C_3F_7NO scattered from MgO(100) and GaAs(100), rotational distributions and spin–orbit ratios were also measured as a function of T_s. The information presented for i-C_3F_7NO/MgO(100) is additional and complementary to a previous detailed study of this system.[1]

Using light- and heavy-atom-scattering and Auger spectroscopy, we probe surface conditions, structurally and chemically, over the temperature range explored for each target crystal, and show that MgO(100), GaAs(100), and Ag(111) are stable surfaces. We discuss and compare the two main mechanisms that can be associated with the experimental findings, namely, electronic and/or phononic molecule–surface interactions, and conclude that the coupling of incident i-C_3F_7NO translational and surface vibrational motions is probably responsible for the experimental observations.

II. Experimental Section

The experimental arrangement shown in Figure 1 was described in detail elsewhere,[1] so only a brief description will be given here, emphasizing aspects especially relevant to the present experiments. A pulsed molecular beam of i-C_3F_7NO seeded in H_2 or He was accelerated to incident kinetic energies of $1 \leq E_{incident} \leq 5$ eV. The beam was skimmed and collimated before entering the ultrahigh vacuum (UHV) surface scattering chamber (base pressure 5×10^{-10} Torr) and was scattered from single-crystal MgO(100), GaAs(100), or Ag(111) surfaces. Nascent NO fragments were detected state-selectively by two-photon, two-frequency laser ionization via the $A^2\Sigma^+ \leftarrow X^2\Pi$ γ system. Ions were produced with several microjoules of 224–227-nm radiation for the resonant transition, and ~1 mJ near 280 nm for the ionizing transition, and were detected with a Channeltron. Signals were collected at or near the specular angle of 45°.

Two quadrupole mass spectrometers (QMS) were used for measuring angular scattering distributions and time-of-flight (TOF) spectra. With the exception of the laser-based optical probe, the scattering–detection arrangement is that of fixed detectors and a rotating crystal. One QMS was oriented at 45° relative to the incident molecular beam, 26 cm from the surface, and equipped with a collimator to give 1.1° angular resolution both in and out of the scattering plane. The second QMS was placed-in-line with the incident molecular beam and used for beam diagnostics and as a residual gas analyzer. $E_{incident}$ values were measured by the TOF technique to within ±0.25 eV. In order to obtain surface chemical composition, an Auger spectrometer (PHI 3017 with 0.6% resolution CMA) was installed. The Auger spectrometer was mounted on a translator with a 7.5-cm retraction travel and was positioned at 135° relative to the incident molecular beam.

Surface quality and characteristics were probed by (1) He diffraction, which is a sensitive probe for structural changes at the topmost surface layer, (2) heavy particle scattering by Xe ($E_{incident}$ = 2.1 eV),[1] which probes a different part of the molecule–surface interaction potential than does He, but may provide a relevant surface diagnostic for the large, heavy molecules at hyperthermal incident kinetic energies required for CID, and (3) Auger spectroscopy.

Cleaved MgO(100) (Atomergic, 10 mm × 10 mm × 1 mm) was aligned, annealed, and characterized as before[6] and was usually cleaned by resistive heating up to 1000 K. Occasionally, the surface was cleaned by cycles of Ar atom bombardment (FAB-Ion Tech, 40 μA, 6 kV, 2–5 min.), followed by thermal annealing. With this procedure, reliable He diffraction patterns were obtained, although they are superimposed on a substantial component of incoherent elastic background, typical of cleaved surfaces.[7,8] Hyperthermal Xe scattering produced relatively sharp (i.e., 16° FWHM), background-free angular distributions near the specular angle. Auger spectroscopy revealed small amounts of carbon (1.4%) and sulfur (3.6%). Argon atom bombardment enabled us to decrease the small amounts of these impurities down to the detection limit, but introduced a trace amount (0.15%) of implanted Ar. Even though MgO is highly insulating, we did not encounter any special problems in obtaining high signal-to-noise (S/N) spectra at low (1–5 μA) beam currents. An important point when the scattered-beam experiments are compared with Auger spectra is the different surface area sampled by the molecular beam (2 mm × 6 mm) as compared with the focused electron beam (0.1 mm × 0.1 mm). We carefully checked for any variations in the Auger spectra for a number of different positions of the electron beam on the surface. No significant variations were found in the relative concentrations of either the carbon or sulfur impurities, or the oxygen or magnesium.

GaAs(100) surfaces (Semia, semiinsulating, 5 cm diameter × 450 μm thickness) were obtained X-ray analyzed (±0.5°) and polished to optical flatness. Crystals were cleaved into approximately 10 mm × 12 mm rectangles. Prior to mounting, the crystals were treated with a solution of (5:1:1) H_2SO_4, 30% H_2O_2, and H_2O for 1–2 min, then rinsed with deionized water, and dried with a stream of ultrahigh-purity helium. In order to avoid redesign of the surface holder, the thin GaAs samples were mounted on top of a 1-mm-thick MgO crystal. Once in vacuum, a crystal was annealed at 775–825 K for ~20 min and characterized by Auger spectroscopy and He and Xe scattering. Although the melting temperature of GaAs is 1511 K, crystal annealing above ~970 K was avoided due to the preferential loss of As and subsequent restructuring of the surface.[9] Likewise, Ar bombardment was avoided due to the preferential sputtering of As.[10] The angular scattering of both He and Xe was broad and bimodal, with a peak near the specular angle (25°), and a backscattered peak at 50°. The angular positions and widths of the scattered distribution of hyperthermal atoms has been shown to be sensitive to the topography or structure of surfaces, and the in-plane scattering of hyperthermal Xe atoms from strongly corrugated surfaces [e.g., GaAs(110)] has exhibited similar bimodal structure.[11] Auger spectroscopy revealed significant

(5) (a) Rettner, C. T.; Fabre, F.; Kimman, J.; Auerbach, D. J. *Phys. Rev. Lett.* **1985**, *55*, 1904. (b) Rettner, C. T.; Kimman, J.; Fabre, F.; Auerbach, D. J.; Morawitz, H. *Surf. Sci.* **1987**, *192*, 107.

(6) Kolodney, E.; Baugh, D.; Powers, P. S.; Reisler, H.; Wittig, C. *Chem. Phys. Lett.* **1988**, *145*, 177.
(7) Rieder, K. H. *Surf. Sci.* **1982**, *118*, 57.
(8) Kolodney, E.; Amirav, A. *Surf. Sci.* **1985**, *155*, 715.
(9) Ekwelundu, E. C.; Ignatiev, A. *J. Vac. Sci. Technol. A* **1988**, *6*, 51.
(10) Singer, I. L.; Murday, J. S.; Cooper, L. R. *Surf. Sci.* **1981**, *108*, 7.

amounts of carbon (18%) and oxygen (22%), and a small amount of sulfur (5%), which did not diminish after thermal annealing. Carbon, oxygen, and sulfur are typical contaminants for fresh GaAs samples.[9] Since Auger sensitivity factors are not accurately known,[12] the error in the reported surface concentrations is estimated to be ±20%.

Before the polished single-crystal Ag(111) surface (Aesar, 10 mm diameter × 2.5 mm thickness) was mounted, it was rinsed with acetone and ethanol after being cleaned with trichloroethylene in an ultrasonic cleaner. Once inside the scattering chamber, it was annealed at 700–1000 K for several hours. No impurities were seen within our detection limit with Auger spectroscopy, and both He and Xe scattering produced sharp, background-free angular distributions of 20 ± 5° FWHM at the specular angle.

T_s was varied in the range 300–1000 K by using a resistive heater (0.25-mm Ta wire in alumina) embedded in the molybdenum surface holder. A double radiation shield made of tantalum enveloped the surface holder. For MgO(100), temperatures were usually measured from the molybdenum surface clamps, which were in good thermal contact with the surface, using a chromel–alumel thermocouple. In order to check any discrepancy between the temperature at the surface and the reading at the clamps, a second thermocouple was attached to the face of a MgO(100) crystal with high-temperature ceramic adhesive (Aremco, 571). This thermocouple reading was compared to a simultaneous reading from the thermocouple attached to one of the surface clamps. There was little or no discrepancy, ΔT, between the surface and clamp temperatures for low temperatures (300–500 K), but ΔT increased nonlinearly with increasing temperature. At the highest T_s (835 K), the clamp temperature reading was 965 K. A polynomial fit to the data was used to convert any temperatures measured at the clamp to T_s values. For GaAs(100), the thermocouple was fastened to the back of the crystal with high-temperature ceramic adhesive, on a portion which slightly overhung the molybdenum surface holder. For Ag(111), the thermocouple was pressed into a 0.8 mm diameter × 1.2 mm hole drilled into the side of the crystal and anchored with ceramic adhesive. Overall, we estimate that T_s is uncertain by only ±10 K.

III. Results

A. i-C_3F_7NO/MgO(100). Figure 2 shows the dependence of the CID yield of i-C_3F_7NO scattered from MgO(100) for $470 \leq T_s \leq 760$ K, and $1.6 \leq E_{incident} \leq 5.0$ eV. At $T_s > 760$ K, a strong ion background originating from the surface holder and heating filament interfered with the signal. The lower T_s limit ensured surface cleanliness and prevented i-C_3F_7NO adsorption during the course of an experiment. It was verified, by Auger spectroscopy, that no long-term adsorption occurred for $T_s \geq 300$ K. Relative and absolute CID yields were calculated as described in detail in a previous publication.[1] Briefly, for each T_s and $E_{incident}$ value we measure the NO fragment density (laser-based detection), summed over internal states and scattering angles. Note that the density-to-flux transformation was not carried out due to insufficient information about the scattered product velocities. Absolute values for CID yields were derived by scaling each of the relative C_3F_7NO yields to the corresponding signal from an NO reference beam (also summed over internal states and scattering angles). All measurements and procedures for extracting rotational distributions and measuring T_s dependences were checked in the scattering chamber with 300 K NO ambient gas or the scattered NO reference beam, under the same conditions and configuration as when detecting NO from CID. It was found that the ambient NO reference signal intensity was practically independent of T_s up to 650 K and then decreased monotonically with increasing T_s due to experimental difficulties deriving from thermally generated ions emanating from the sample holder. At 760 K, the signal was smaller by 30%. Consequently, a small correction factor was introduced for CID yields obtained at the highest T_s values.

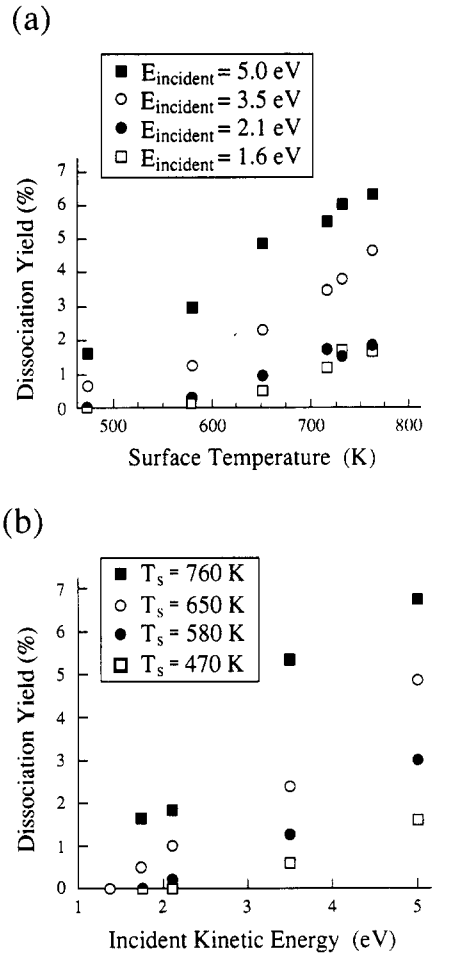

Figure 2. (a) CID yield (±50% absolute uncertainty) of i-C_3F_7NO/MgO(100) scattering vs T_s (±10 K) for several $E_{incident}$ values. A small correction (described in the text) was applied to the $T_s > 650$ K values. (b) CID yield (±50% absolute uncertainty) of i-C_3F_7NO/MgO(100) scattering vs $E_{incident}$ (±0.25 eV) at several T_s values (±10 K).

Relative and absolute CID yields were determined as follows. Relative CID yields were obtained by measuring the NO fragment density, summed over internal states, for different $E_{incident}$ and T_s values. Since the NO state distributions obtained over scattering angles of 25–45° (8° resolution) were similar, and the angular distributions for scattered NO and i-C_3F_7NO were also similar, we concluded that detailed integration over scattering angles was unnecessary. The incident i-C_3F_7NO beam flux was usually kept constant, with measurements at different $E_{incident}$ performed at a $[i\text{-}C_3F_7NO]/[H_2]$ ratio of 1:300. Incident fluxes were estimated from the nozzle throughput and by measuring relative i-C_3F_7NO signal intensities in the scattering chamber with a QMS on the incident beam line. $E_{incident}$ was adjusted by adding Ar or He while keeping the nozzle throughput constant. As a check, we also used gas mixtures with different $[i\text{-}C_3F_7NO]/[H_2]$ ratios (1:125–1:650) to achieve the same final velocities, and there was good agreement between the two sets of measurements. The uncertainty in the relative CID yields is estimated to be ±20%. The NO contamination percentage in the incoming i-C_3F_7NO beam and its relative contribution to the total scattered NO signal (CID product) was found to be negligible.

When absolute CID yields were determined, a reference NO beam with well-controlled incident flux was used for calibration. The NO and i-C_3F_7NO relative incident fluxes were measured both in the source chamber and in the scattering chamber. The NO flux was either equal to the i-C_3F_7NO flux or in a well-known ratio. Aerodynamic focusing (far-field enrichment of the beam center with the heavy molecule) was estimated experimentally by comparing incident beam flux ratios in the source and scattering

(11) Amirav, A.; Cardillo, M. J.; Trevor, P. L.; Lim, C.; Tully, J. C. *J. Chem. Phys.* **1987**, *87*, 1796.
(12) *Handbook of Auger Electron Spectroscopy*, 2nd ed.; Physical Electronics Division, Perkin-Elmer Corp.: Eden Prairie, MN, 1978.

chambers, and approximate enrichment ratios for i-C_3F_7NO-seeded beams with respect to the NO reference beam were obtained. For given $E_{incident}$ and T_s, the NO photoionization signals from the scattered NO beam and the fragment NO from the CID experiments were separately measured, with all other experimental parameters held constant. After integration over the NO internal-state distributions was performed for both beams, the flux-normalized ratio of the CID NO signal to the NO reference signal gave the absolute dissociation yield. Reference NO calibration measurements were performed separately for each $E_{incident}$, and all CID yields represent an average of data taken over an extended period of time. The uncertainty in the absolute CID yields is estimated to be ±50%.

As mentioned above, CID yields result from the measurement of NO fragment densities. Product density-to-flux transformations are not carried out, as the different scattered velocity distributions associated with NO fragments with different internal states are unknown. Therefore, since molecular cross sections in the center-of-mass (cm) frame are related to scattered flux, we are not able to calculate dissociation probabilities. The situation is complex, since the decomposition of a molecule that has rebounded from the surface sends fragments recoiling into many angles in the molecule-based cm system. Even if the products are scattered isotropically in the cm system, the rebounding cm system moves anisotropically in the laboratory, with ranges of speeds and angles that depend on $E_{incident}$, θ_s, T_s, etc. Furthermore, the scattered i-C_3F_7NO molecules exhibit a distribution of internal states, and i-$C_3F_7NO^\dagger$ decomposition at a given $E^\dagger$ produces NO in a number of internal states, each of which has a distribution of translational energies. Moreover, these distributions may differ from one NO state to the next (e.g., high J'' may be associated with lower cm translational energies). Also, since scattered molecules have less translational energy than when incident, the spatial density of the scattered molecules will increase, particularly for molecules that decompose. This bunching effect is likely to vary with $E_{incident}$ and will be most severe at the threshold region. Therefore, near threshold, relative CID probabilities are probably smaller than the corresponding yields. On the other hand, molecules excited to $E^\dagger$ slightly above D_0 have long lifetimes and may not all dissociate before reaching the detector, so the measured yield may not reflect all of the molecules that are *destined* to dissociate. Thus, CID probabilities probably increase more rapidly with $E_{incident}$ than CID yields, especially near threshold. A more detailed discussion is given in ref 1.

It is obvious from Figure 2 that CID yields increase strongly with both $E_{incident}$ and T_s. Moreover, the $E_{incident}$ threshold for CID is a function of T_s. The experimental threshold for i-C_3F_7NO CID is 2.4 ± 0.20 eV at 470 K, <2.0 eV at 580 K, and <1.6 eV at 650 K (D_0 = 1.64 eV for i-$C_3F_7NO \rightarrow i$-C_3F_7 + NO). We attempted to see if a larger energy gap between D_0 and $E_{incident}$ (0.34 eV) could be bridged by the T_s contribution but found no observable CID signal for $E_{incident}$ = 1.3 eV and T_s up to 650 K.

Interestingly, we found no pronounced or systematic dependence of NO internal excitation (rotational, electronic, and vibrational) on either $E_{incident}$ or T_s. Since the $E_{incident}$ dependence was described previously,[1] we will describe here in some detail the T_s dependence. Over the temperature range studied, the rotational distributions depend only weakly on T_s. Figure 3 shows the very similar rotational distributions for i-C_3F_7NO at $E_{incident}$ = 5.0 eV, for T_s = 580 K and T_s = 780 K. The results for other combinations of $E_{incident}$ and T_s were essentially the same. If the distributions are assigned rotational "temperatures", typical T_{rot} for the upper $^2\Pi_{3/2}$ spin–orbit state is ~500 K, whereas for the lower $^2\Pi_{1/2}$ spin–orbit state it is ~380 K, decidedly lower than T_s. Also note that the spin–orbit ratio obtained via CID ($[^2\Pi_{3/2}]/[^2\Pi_{1/2}]$ = 0.36) is smaller than that for NO thermalized at 300 K and changes little with T_s. The insensitivity of the rotational distributions and spin–orbit ratio to T_s provides further evidence for the direct, impulsive nature of the scattering process. We did not observe NO(v''=1) in the γ (1–1) region, with $E_{incident}$ = 5.0 eV and T_s = 580–760 K. Assuming similar spin–orbit and rotational distributions in v'' = 0 and v'' = 1, and taking into account the different Franck–Condon factors, an upper limit of ~2% could be placed on the $[v''=1]/[v''=0]$ ratio.

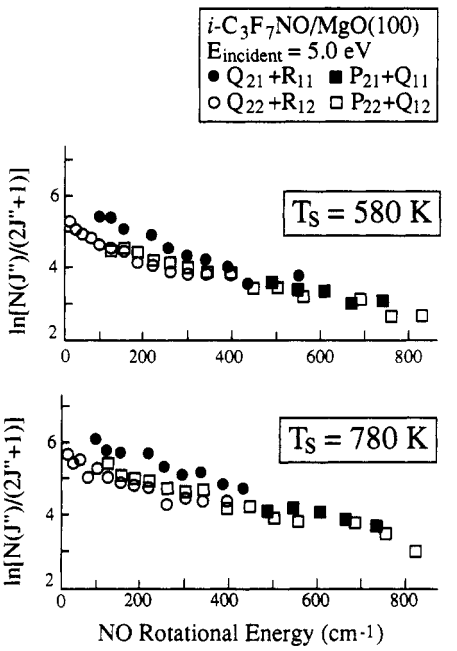

Figure 3. Rotational distributions (Boltzmann plots) for the NO dissociation product following scattering of i-C_3F_7NO from MgO(100) at $E_{incident}$ = 5.0 eV, for T_s = 580 and 780 K. Each distribution represents an average of several different measurements. Filled and empty symbols indicate rotational populations of $^2\Pi_{1/2}$ and $^2\Pi_{3/2}$ NO spin–orbit states, respectively.

We carefully checked for changes of the surface structure and stoichiometry upon heating, which could influence the CID yields. He diffraction gave no indication of surface reconstruction upon heating.[8] This was also shown by LEED studies[13] on MgO annealed at temperatures up to 1400 K, where it was found that less stable planes undergo thermal faceting into (100) planes. It should be mentioned that when they do occur, surface rearrangements in oxide ceramics are usually induced by chemical changes in stoichiometry. For a cubic rock salt crystal like MgO, the (100) plane is electrically neutral, with no net dipole moment, and is therefore a low-energy and very stable surface. Similarly, we scattered NO, hyperthermal Xe, and i-C_3F_7NO from MgO(100) over this temperature range and did not observe any qualitative changes in the shape of the near-specular scattered lobe besides small broadening effects.

Due to the highly insulating nature of MgO (bulk optical band gap of 7.8 eV),[14] there is only limited information available about its surface electronic structure. Surface-sensitive electron spectroscopies such as UPS, XPS, and EELS[15] applied to the (100) face indicated a valence band structure similar to the bulk one, but with an optical band gap smaller by 1.5–2.0 eV. In this context, one has also to consider the abundances of point defects on rock salt oxide surfaces and their electronic structure, which is generally unknown. The two common ones are an O atom deficiency (F_s center) and a Mg atom deficiency (V_s center).[15] A surface defect state at 2.3 eV has been identified from EELS measurements of a UHV-cleaved MgO(100) surface, which disappeared after exposure to O_2 or thermal annealing.[14] This 2.3-eV transition could also be generated by electron or ion bombardment. Although known to be a surface defect state, it is unclear as to whether an F_s center or a V_s center is involved. Also, the magnitude of electron energy loss peak was larger than expected from the surface defect density suggested from the MgO(100) LEED patterns.

(13) Henrich, V. E. *Surf. Sci.* **1976**, *57*, 385.
(14) Kingery, W. D., Ed. *Advances in Ceramics, Structure and Properties of MgO and Al_2O_3 Ceramics*; American Ceramic Society: Columbus, OH, 1984; Vol. 10.
(15) Henrich, V. E. *Rep. Prog. Phys.* **1985**, *48*, 1481.

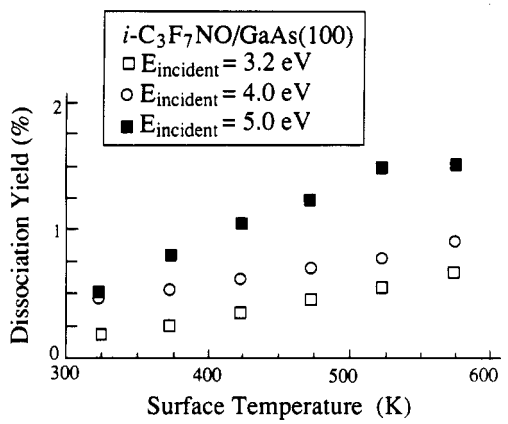

Figure 4. Dissociation yield (±50% absolute uncertainty) of i-C_3F_7NO scattered from GaAs(100) vs T_s (±10 K) for several $E_{incident}$ values.

In order to get detailed information on the chemical composition and possible changes in the stoichiometry at the MgO(100) surface, we obtained Auger spectra in the range 100–1300 eV, at several T_s values. By monitoring the oxygen and magnesium KLL peaks, we found that the [Mg]/[O] ratio was practically independent of T_s in this range, and an accurate measurement showed that the concentration ratio was stable to within ±3%. Repeated measurements were taken between different surface temperatures in order to verify that the surface stoichiometry did not change due to the 3-kV primary electron beam bombardment. We also did not see any chemical shifts (on the order of 2–3 eV) that might indicate the increased involvement of other oxidation states, adsorbed species, or electronic surface states. A few other very weak Auger features observed were a line at 1250 eV, which might be associated with a KLL transition from unoxidized Mg,[16] and occasionally a small amount of carbon. No correlation was found between the intensities of these peaks and the temperature dependence of the CID yield and NO internal excitations. In summary, as expected on the basis of the stability of the MgO(100) surface, we found no evidence for structural or chemical changes in the range of $300 \leq T_s \leq 1000$ K.

B. i-C_3F_7NO/GaAs(100) and i-C_3F_7NO/Ag(111). The absolute CID yields for both GaAs(100) and Ag(111) were lower than that for MgO(100). Although the i-C_3F_7NO/Ag(111) signal was too small to yield meaningful NO rotational distributions from CID, comparisons between i-C_3F_7NO/MgO(100) and i-C_3F_7NO/GaAs(100) can be made. In particular, there is a strong dependence on both T_s and $E_{incident}$ for the CID of i-C_3F_7NO scattered from GaAs(100). As shown in Figure 4, CID depends strongly on both $E_{incident}$ and T_s. At the lowest T_s of 300 K, we saw no evidence for trapping–desorption in the scattering of Xe, NO, or i-C_3F_7NO. Also, Auger spectroscopy revealed no evidence of long-term adsorption. As with i-C_3F_7NO/MgO(100) we did not find any discernible dependence of the internal excitation of the NO fragment on either $E_{incident}$ or T_s. For the ranges of $E_{incident}$ and T_s studied, the spin–orbit ratio, $[^2\Pi_{3/2}]/[^2\Pi_{1/2}]$, is lower than that of 300 K NO and similar to that produced from i-C_3F_7NO/MgO(100) CID. Different NO rotational distributions were obtained for each spin–orbit state, with the $^2\Pi_{3/2}$ state consistently exhibiting higher rotational excitation than the $^2\Pi_{1/2}$ state. Except for minor differences, NO rotational distributions from the CID of i-C_3F_7NO scattered from GaAs(100) and MgO(100) were similar. A Boltzmann plot of the NO rotational distribution for i-C_3F_7NO/GaAs(100) CID is shown in Figure 5. Under otherwise identical conditions, the CID yield for i-C_3F_7NO scattered from GaAs(100) is approximately a factor of 2 smaller than for i-C_3F_7NO/MgO(100).

The lack of significant change in the scattering behavior for either NO, hyperthermal Xe, or i-C_3F_7NO scattered from either GaAs(100) or Ag(111) suggests the absence of surface-structure

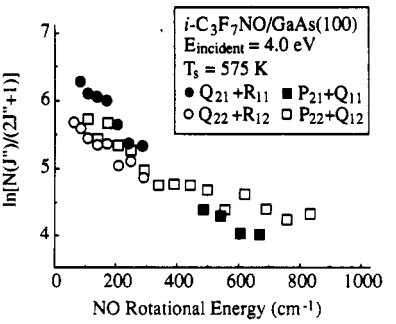

Figure 5. Rotational distribution (Boltzmann plot) for the NO CID product following i-C_3F_7NO/GaAs(100) scattering at $E_{incident}$ = 4.0 eV and T_s = 575 K. The distribution represents an average of several different measurements. Filled and empty symbols indicate rotational populations of $^2\Pi_{1/2}$ and $^2\Pi_{3/2}$ NO spin–orbit states, respectively.

TABLE I: Comparison of i-C_3F_7NO CID Yields at $E_{incident}$ = 4.0 eV and T_s = 580 K for the Different Surfaces

surface	CID yield, %	Θ_{SD},[a] K
MgO(100)	1.8	540
GaAs(100)	0.9	250
Ag(111)	0.5	155

[a] Θ_{SD} is the estimated surface Debye temperature.

and stoichiometry change upon heating. For GaAs(100), Auger spectroscopy in the range of 100–1300 eV, at two different surface temperatures, exhibited only very minor changes in concentration. For Ag(111), Auger spectra showed no impurities, within our detection limit, for T_s ranging from 300 to 800 K.

For i-C_3F_7NO/Ag(111) at $E_{incident}$ = 4.0 eV and T_s = 580 K, the CID yield is roughly 4 times smaller than for i-C_3F_7NO/MgO(100). The CID signal increased slightly but steadily with T_s over the range 300–800 K. Even at the highest T_s values, the CID signal from dissociative scattering from Ag(111) was small. CID yields for MgO(100), GaAs(100), and Ag(111) surfaces, for $E_{incident}$ = 4.0 eV and T_s = 580 K, are compared in Table I.

IV. Discussion

In discussing dynamical mechanisms that are consistent with the experimental observations, we consider molecule–surface charge-transfer processes and impulsive collisional coupling to surface vibrations. Note that we have already established the stability of the surfaces, finding no evidence for structural or chemical changes over the temperature ranges probed for each crystal. Furthermore, the impulsive nature of the molecule–surface collision in the hyperthermal energy regime probably makes the observed dynamics relatively insensitive to morphological details of the surface. Therefore, even if some structural or chemical changes occurred that we did not detect, they are not expected to be mechanistically dominant.

Molecule–surface charge-transfer processes, such as hyperthermal surface ionization, have been observed experimentally in previous hyperthermal surface scattering experiments.[3] Although surface ionization yields are normally extremely small for organic molecules and moderate surface temperatures, Danon and Amirav found that at the highest incident kinetic energies used in their experiments ($1 \leq E_{incident} \leq 12$ eV), the ion yields for these systems could be increased dramatically. However, absolute ion yields are still usually less than 1% and exhibit only a weak T_s dependence.[3] Hyperthermal surface ionization and other molecule–surface charge-transfer processes have been dealt with theoretically in terms of harpooning and the temporary formation of ions.[17] A similar electronic mechanism was also suggested for photodesorption experiments of NO on Pt foil and Pt(111)[18,19] and used

(16) Bassett, P. J.; Gallen, T. E.; Prutton, M.; Matthew, J. A. D. *Surf. Sci.* **1972**, *33*, 213.

(17) (a) Gadzuk, J. W.; Holloway, S. *J. Chem. Phys.* **1986**, *84*, 3502. (b) Gadzuk, J. W.; Holloway, S. *Chem. Phys. Lett.* **1985**, *114*, 314. (c) Holloway, S.; Gadzuk, J. W. *Surf. Sci.* **1985**, *152*, 838.

(18) Burgess, D., Jr.; Cavanagh, R. R.; King, D. S. *J. Chem. Phys.* **1988**, *88*, 6556.

to explain the substantial vibrational excitation observed in NO/Ag(111) direct inelastic scattering at high T_s, where it was shown that the density of accessible electronic states in the metal has the same exponential temperature dependence as the vibrational excitation probability.[5] Taking the Fermi level for MgO at the top of the O(2p) valence level and placing the vacuum energy coincident with the bottom of the conduction band, the electronic work function of MgO(100) would be ~6.2 eV, making strong coupling to the surface electronic states unlikely. However, if thermal annealing did not reduce the density of the possible surface defect state at 2.3 eV to negligible levels, electronic coupling of the incident molecule to this defect state would be possible. If this were the case, the surface defect density and the CID yields would be expected to depend on the preparation and condition of the surface. However, the CID yield for i-C_3F_7NO scattered from a MgO(100) surface roughened by fast Ar bombardment was less than or equal to the CID yield observed both before Ar bombardment and after thermal annealing of the roughened surface. Due to the different scattering behavior for the rough and smooth surfaces, angular integration was performed in order to compare the CID yields. The change in surface structural order for both conditions was verified with He and Xe scattering.

As another check, we monitored NO($v''=1$) following NO/MgO(100) collisions at high T_s, assuming that NO($v''=1$) production in high-T_s collisions may reflect the importance of the electronic mechanism. No NO($v''=1$) was observed up to $E_{incident}$ = 0.90 eV and T_s = 775 K, with an upper limit of $[v''=1]/[v''=0] \leq 0.001$. This is smaller by more than 1 order of magnitude than the vibrational excitation probability reported for NO/Ag(111) scattering under similar conditions[5] and should also be compared with a ~3% probability expected for thermal equilibration with an 775 K surface. The experimentally determined work function for Ag(111) is 4.47 eV.[20] These findings are in contrast with what would be expected for a mechanism based on molecule–surface charge transfer.

One of the most striking observations in the present CID measurements is the smaller dissociation yield for i-C_3F_7NO scattered from GaAs(100) (bulk bandgap 1.423 eV)[21] and Ag(111) than from MgO(100). In the absence of large low-energy MgO(100) surface defect densities, larger CID yields would be expected for scattering from the silver surface if molecule–surface charge transfer was the dominant CID mechanism.

Thus, we are led to propose that coupling of the incoming molecule to surface vibrational motions is a possible explanation for the effect of surface temperature on the CID yield. In a more detailed previous publication,[1] we presented experimental findings for the CID of n- and i-C_3F_7NO scattered from MgO(100), which led us to favor a statistical mechanism involving collision-induced vibrational excitation within the S_0 and/or T_1 electronic manifolds of n,i-C_3F_7NO, followed by intramolecular vibrational redistribution and statistical unimolecular decomposition. For the CID of i-C_3F_7NO after impulsive scattering from both MgO(100) and GaAs(100), the NO rotational distributions vary only weakly with $E_{incident}$ and T_s, while the CID yields rise dramatically. This suggests that the severe distortion of the nuclear framework of the incident molecules upon collision with the surface creates a scattered ensemble with a broad internal energy distribution.

According to the above picture, the measured CID yield is in some way proportional to the integral of the i-C_3F_7NO vibrational energy distribution, $P(E_v)$, above a reaction threshold, $E_{th} = D_0 + \Delta E$, where ΔE accounts for molecules that pass through the detection region before reacting. Thus for molecules in the high-energy tail of a broad $P(E_v)$ distribution, the distribution of molecules above E_{th} is weighted toward energies that are just above E_{th}. The influence of T_s may be to broaden the distribution of collision energies, in a way analogous to the spreading caused by target thermal motion in beam-gas collisions.[22] Increasing T_s increases surface phonon excitation and, consequently, this energy spread. Thus, in contrast to increasing $E_{incident}$, which shifts the $P(E_v)$ maximum to higher energy, increasing T_s may broaden $P(E_v)$. This would increase the CID yield by increasing the integral of $P(E_v)$ above E_{th} and explain why NO distributions exhibit near-threshold behavior for all $E_{incident}$ and T_s.

Except for the CID yields, the i-C_3F_7NO/MgO(100) and i-C_3F_7NO/GaAs(100) systems behave similarly, suggesting the possibility of a common mechanism. Because of the large size of i-C_3F_7NO, corrugation differences between the surfaces are not expected to play an important role in the dynamics. The main difference is the higher CID yield for scattering from MgO(100), which is probably due to the higher efficiency of i-C_3F_7NO translational to internal energy transfer with this stiff surface. For mushier surfaces (i.e., lower Debye temperatures), one expects less distortion of the incoming molecule than in the case of a hard wall, resulting in less vibrational excitation in scattered molecules. The estimated surface Debye temperature, Θ_{SD}, is 540 K for MgO(100),[23] 250 K for GaAs(100),[24] and 155 K for Ag(111).[25] Note that the CID yields for i-C_3F_7NO shown in Table I approximately scale as their respective Θ_{SD} values.

Similarly, the efficacy of energy transfer to the crystal is greater for less stiff surfaces, possibly competing with conversion of $E_{incident}$ to i-C_3F_7NO vibrational energy. In heavy-atom scattering, large $E_{incident}$ losses in the direction of the surface normal have been observed for Xe scattering from both Ag(100) and GaAs(110).[11] Also, it was noted that Hg/MgO(100) and I_2/MgO(100) energy transfer to lattice vibrations was smaller than for Xe/Ag(100) and Xe/GaAs(110), despite the much heavier Hg and I_2 colliders.[26,27] Furthermore, surface temperature had no effect on the energy transferred from I_2 incident kinetic energy to MgO(100) lattice motions[26] and exhibited negligible (<10%) energy transfer to diamond,[11] which has a bulk Debye temperature 2.3 times higher than MgO(100).[28] For i-C_3F_7NO, it is reasonable that a larger fraction of $E_{incident}$ is lost to surface phonons for Ag(111) and GaAs(100) than for MgO(100). The fact that the CID yield is smallest for Ag(111) and largest for MgO(100) is qualitatively consistent with the different anticipated distortions of the C_3F_7NO nuclear frame and the relative energy-transfer efficiencies to the crystal lattice.

V. Summary

i-C_3F_7NO molecules were expansion-cooled and aerodynamically accelerated to $E_{incident}$ = 1–5 eV and scattered impulsively from well-characterized MgO(100), GaAs(100), and Ag(111) single-crystal surfaces under UHV conditions. The T_s dependence of the resulting CID was studied for $300 \leq T_s \leq 760$ K.

A fraction of the scattered molecules have internal vibrational excitation that exceeds D_0, and CID is verified unambiguously by detecting NO state-selectively with two-photon, two-frequency laser ionization. CID yields increase markedly with both $E_{incident}$ and T_s, whereas NO rotational distributions are relatively insensitive to $E_{incident}$ and T_s.

We have no proven model, but rationalize the effect of surface temperature on the CID yield by the interaction of the incoming molecule with surface phonons. Increased phonon excitation at

(19) Buntin, S. A.; Richter, L. J.; King, D. S.; Cavanagh, R. R. *J. Chem. Phys.* **1989**, *91*, 6429.
(20) Cardwell, A. *Phys. Rev.* **1953**, *92*, 554.
(21) Williams, R. E. *Gallium Arsenide Processing Techniques*; Artech House, Inc.: Dedham, MA, 1984.
(22) van der Zande, W. J.; Zhang, R.; Zare, R. N. Collisional Energy Spread in Hot Atom Reactions Caused by Thermal Motions of the Reagents. In *Spectral Line Shapes*; Frommhold, L., Keto, J. W., Eds.; V6 AIP Conference Proceedings 216; A. Deepak Pub.: New York, 1990; pp 301–310.
(23) (a) Brusdeylins, G.; Doak, R. B.; Skofronick, J. G.; Toennies, J. P. *Surf. Sci.* **1983**, *128*, 191. (b) Barron, T. H. K.; Berg, W. T.; Morrison, J. A. *Proc. R. Soc. London* **1959**, *250*, 70.
(24) (a) Blakemore, J. S. *J. Appl. Phys.* **1982**, *53*, R123. (b) Holste, J. C. *Phys. Rev. B* **1972**, *6*, 2495.
(25) Goodman, R. M.; Farrell, H. H.; Somorjai, G. A. *J. Chem. Phys.* **1968**, *48*, 1046.
(26) Kolodney, E.; Amirav, A. *Chem. Phys. Lett.* **1984**, *111*, 366.
(27) (a) Kolodney, E.; Amirav, A. *Surf. Sci.* **1984**, *148*, 153. (b) Kolodney, E.; Amirav, A.; Elber, R.; Gerber, R. B. *Chem. Phys. Lett.* **1984**, *113*, 303.
(28) *American Institute of Physics Handbook*, 3rd ed.; McGraw-Hill: New York, 1982.

the surface as T_s is increased may serve to increase the effective collisional energy spread, thus broadening the i-C_3F_7NO vibrational energy distribution and increasing the CID yield. Clearly, calculations as well as additional experiments are needed, and future experiments in our laboratory will involve measurements of the velocity distribution of the dissociated and undissociated scattered molecules.

Acknowledgment. We thank J. Crane, A. Amirav, B. Koel, C. Mak, S. G. Hummel, P. D. Dapkus, and D. Baugh for stimulating and helpful discussions. We especially thank S. G. Hummel and P. D. Dapkus for providing GaAs(100) samples.

Registry No. *iso*-C_3F_7NO, 422-98-0; MgO, 1309-48-4; GaAs, 1303-00-0; Ag, 7440-22-4; NO, 10102-43-9.

Photochemical Pathways of Water on Pd(111) at 6.4 eV

X.-Y. Zhu, J. M. White,*

Department of Chemistry, University of Texas, Austin, Texas 78712

M. Wolf, E. Hasselbrink,* and G. Ertl

Fritz-Haber-Institut der Max-Planck-Gesellschaft, D-1000 Berlin 33, Faradayweg 4-6, FRG
(Received: March 27, 1991; In Final Form: June 24, 1991)

The photochemistry of water adsorbed on Pd(111) was studied by high-resolution electron energy loss spectroscopy (HREELS), temperature-programmed desorption (TPD), and time-of-flight (TOF) mass spectroscopy. UV laser irradiation (6.4 eV, 193 nm) of the water bilayer adsorbed on Pd(111) results in sequential dissociation to form surface hydroxyl groups first and later atomic oxygen. The first step is dominating for irradiation with up to 2×10^{18} photons/cm^2. In this case the dissociating hydrogen atom is retained on the surface. For prolonged irradiation the second step is observed accompanied by recombination of a dissociating hydrogen atom with a surface hydroxyl group leading to the desorption of molecular water. Beside these processes also direct desorption of molecular water is observed dominating the desorption yield during the initial stage of irradiation. In both cases water desorption is nonthermal, with a mean translational energy, $\langle E_{trans} \rangle / 2k$, of (600 ± 60) K. On c(4×2)CO and p(2×2)O covered Pd(111), only direct photodesorption is observed, with cross sections of (2.4 ± 0.1) × 10^{-20} cm^2 and (2.6 ± 0.3) × 10^{-20} cm^2, respectively. The photochemistry is attributed to transient attachment of photoexcited substrate electrons.

Introduction

As part of the continuing effort to understand the chemistry and physics of photoinduced processes at the adsorbate–metal interfaces, Wolf et al. recently studied the dynamics of the UV photochemistry of water adsorbed on Pd(111).[1,2] Both molecular desorption, studied by time-of-flight (TOF) spectroscopy, and adsorbate-state conversion, shown in temperature-programmed desorption (TPD), were observed. The latter effect was attributed to photodissociation of water on the surface. Comparison of H_2O and D_2O showed strong variations of desorption and conversion cross sections with isotope substitution. However, due to a lack of means to directly identify the chemical species on the surface during irradiation, detailed understanding of the photoreaction pathways was still missing.

The adsorption of water on transition-metal surfaces has been extensively studied in the past. A recent elegant review by Thiel and Madey describes in detail the present knowledge and understanding in this field.[3] On many transition-metal surfaces, such as the (111) face of fcc metals, adsorbed water forms an epitaxial "water bilayer" structure, in which water molecules are hydrogen-bonded in hexagonal rings. Alternating molecules in this ring structure have their oxygen lone pair electrons pointing toward the surface. The intervening molecules are hydrogen bonded to these lower molecules and are raised by ~1 Å from the surface. It is believed that such a bilayer structure is also formed on Pd(111). The saturation coverage of this structure is two-thirds of a monolayer (ML) (H_2O to surface metal atom ratio).

Water is transparent, in either vapor or ice form, for near-UV irradiation ($h\nu \leq 6.6$ eV, $\sigma \leq 10^{-20}$ cm^2).[4,5] Since the geometry and electronic structures of H_2O are only slightly perturbed upon adsorption,[3] we believe that intraadsorbate excitation in H_2O/Pd(111) at 6.4-eV photon energy is unlikely. Our previous polarization study suggests that the photochemistry is initiated by excitation in the substrate.[2]

The present study was undertaken to obtain detailed information concerning the photoreaction pathways of water on Pd(111). For that purpose, high-resolution electron energy loss spectroscopy (HREELS) was used in conjunction with temperature-programmed desorption (TPD) and time-of-flight (TOF) spectroscopy. Upon UV-laser irradiation (193 nm, i.e, 6.4 eV), water dissociates and desorbs. HREELS indicates that photodissociation proceeds via two steps: first the formation of surface hydroxyl groups and later the dissociation of these resulting in atomic oxygen adsorbed on the surface. The latter process is accompanied by desorption of molecular water. The effects of preadsorbed CO and O on the thermal and photochemistry of water have also been investigated.

Experimental Section

The experiments were conducted in two ultrahigh vacuum (UHV) chambers with base pressures of (1–2) × 10^{-10} mbar. The first chamber was pumped by ion, turbomolecular, and Ti sublimation pumps and has been described previously.[6] It houses a LK-2000 spectrometer for HREELS, a UTI-100C quadrupole mass spectrometer for TPD and residual gas analysis (RGA), a PHI hemispherical energy analyzer and a Leybold X-ray source for X-ray photoelectron spectroscopy (XPS), PHI-LEED optics for low-energy electron diffraction (LEED) measurement, a Kratos

(1) Wolf, M.; Nettesheim, S.; White, J. M.; Hasselbrink, E.; Ertl, G. *J. Chem. Phys.* **1990**, *92*, 1509.
(2) Wolf, M.; Nettesheim, S.; White, J. M.; Hasselbrink, E.; Ertl, G. *J. Chem. Phys.* **1991**, *94*, 4609.
(3) Thiel, P. A.; Madey, T. E. *Surf. Sci. Rep.* **1987**, *7*, 221.
(4) Gurtler, P.; Saile, V.; Koch, E. E. *Chem. Phys. Lett.* **1977**, *51*, 386.
(5) Kobayashi, K. *J. Phys. Chem.* **1983**, *87*, 4317.
(6) Zhu, X.-Y.; White, J. M. *J. Chem. Phys.* **1991**, *94*, 1555.

0022-3654/91/2095-8393$02.50/0